Rotating Stall Cells in a Low-Speed Axial Flow Compressor

F. A. E. Breugelmans* and K. Mathioudakis†
von Kármán Institute for Fluid Dynamics, Rhode Saint Genèse, Belgium
and
F. Casalini‡
University of Bari, Bari, Italy

An experimental investigation of the flowfield inside a high hub-to-tip ratio, single-stage compressor is described. Fast-response instrumentation was used for the measurements in the absolute and relative frames of reference. The information was digitized for further analysis of the instantaneous and averaged flow parameters. The calculation of power spectra and the autocorrelation function, and the phase-locked averaging technique are used in this study. This technique consists of dividing the long sample in time intervals equal to the period as obtained by fast Fourier transforms and ensemble averaging these intervals. This procedure has been adopted because it can handle single- and multicell patterns. Two types of perturbation are distinguished: the small eight-cell stall and the single- or double-cell pattern with deep stall. The overall flow behavior, as well as the detailed flowfield structure, are presented for the two cases as measured with stationary probes. On-blade flow measurements suggest the existence of important radial velocities near the rotor blade surface when deep stall occurs.

Nomenclature

B = stability parameter, $= \mu_m / 2\omega L_c$
$E(f)$ = V'^2 for Δf window, $m^2/s^2/Hz$
f = frequency, Hz
f_s = sampling frequency, Hz
h = blade height
IGV = inlet guide vane
L_c = effective compressor length, m
N = sample size
U = peripheral velocity, m/s
V = absolute velocity, m/s
V' = fluctuation velocity $= |\bar{V} - V|$, m/s
α = absolute flow angle from axial, deg
Δf = frequency window, Hz
λ = blockage factor, $= 1 - \bar{V}_a / V_{a,CF}$
ϕ = flow coefficient, $= \bar{V}_a / U_T$
ψ = load coefficient $[P_{static,2} - P_{total,1}] / \frac{1}{2}\rho U_T^2$
ω = Helmholtz resonator frequency

Subscripts

a = axial
c = stall cell
CF = clean flow
e = effective cooling velocity
m = mean radius
T = tip
TS = total to static
1 = upstream; hot wire 1
2 = downstream; hot wire 2
$\bar{\ }$ = average

Introduction

THE aerodynamic and mechanical performance of single- and multistage compressors is seriously influenced by the occurrence of rotating stall. When the compressors are operated at small flow coefficients, a phenomenon occurs which covers the whole or part of the blade span and extends in the circumferential direction. This phenomenon occurs in one or more periodic events called rotating stall cells, rotating at a fraction of the rotor speed. It is important to avoid or delay this phenomenon to make full use of the operating range.

Small-perturbation theories and nonlinear approaches have been used to investigate the onset of rotating stall.[2,3] The compressor was modeled as a cascade or as axisymmetric surfaces. The flowfield itself was not predicted, but some success was obtained in the prediction of number of cells, propagating velocity, and onset of stall. A correlation for stalled compressor performance, assuming a simplified flow model combined with experimental results, has been developed.[4]

Prior experimental investigations were concerned primarily with the overall results such as the number, propagation, and extent of the stall cells.[5] Detailed flow investigations have been reported for the absolute motion and relative frame of reference.[6,7]

The present study primarily covers the absolute flowfield in front of and behind the rotor at different rotating stall conditions occurring in a single-stage compressor and provides information on the flow behavior in the relative motion by measurements on the rotor blade.

Experimental Facility and Instrumentation

The single-stage low-speed compressor used for these experiments is the VKI R-1 facility (Fig. 1). It is an open-loop,

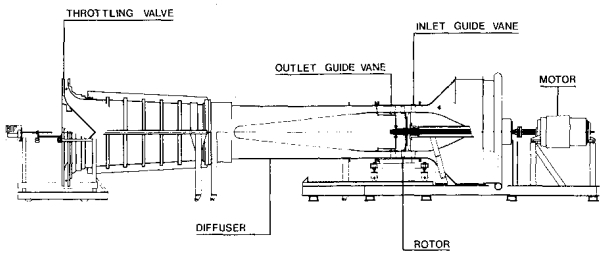

Fig. 1 Low speed axial flow compressor.

Received Aug. 11, 1983; revision received Sept. 14, 1984.

*Head Turbomachinery Department.
†Research Assistant.
‡Associate Professor, University of Bari.

constant annular section facility with an inner diffuser and throttle valve. The rotor is driven by a 55-kW dc motor with a speed control from 0 to 1500 rpm. The outer diameter is 0.704 m (constant) and the hub-to-tip ratio equals 0.78. The number of blades is 39 (IGV), 25 (rotor), and 25 (stator) with a midspan solidity of 1, 1.015, and 1, respectively. The blades are of the NACA 65 series. The blade row spacing was chosen to provide space for axial flow traverses in front of, behind, and between the blade rows. The facility, test section, and blading are documented.[7]

The stage performance is obtained using directional pressure probes of the NACA short prism type positioned 10 mm in front of the IGV and 25 mm downstream of the stator vanes.

The unsteady flow measurements in the stationary frame are performed using two crossed hot-wire probes placed 40 and 30% of the mean blade chord up and downstream of the rotor. The hot wires are 9-μm platinum-plated tungsten wires with a length-to-diameter ratio of 200. Their calibration curves are derived in the form of the ratios Ve_1/Ve_2, $(Ve_1 - Ve_2)/V$ as a function of the angle between wire 1 and velocity vector in the plane of the wires, which is normal to the radial direction.

For measurements near the rotor blade surface, two sensors are utilized; namely, a thermal tuft (Fig. 2a) and a V-shaped hot-wire combination (Fig. 2b). Both are placed at the midchord and midspan positions on the rotor blade during successive experiments (Fig. 2c). The thermal tuft consists of two parallel wires operating at different overheat ratios. Under these circumstances, when the ratio of the two effective cooling velocities is 0.2 the flow is attached to the blade surface and normal to the wires. When the velocity vector becomes more parallel to the wires or small amounts of separation occur the ratio lies between 0.2 and 1.0. Finally, when flow reversal occurs the value is 1.20. The V-shape sensor is operated on the same principle as the crossed hot-wire probes. It is used to measure the velocity magnitude and angle with respect to a reference direction near the blade surface.

All the hot wires are operated at constant temperature using VKI anemometer bridges. A low-noise mercury slip ring (<50 μV) is used to transmit the signal from the hot wires on the rotor to the anemometer bridges connected to a 16 channel data acquisition system. The system contains an amplifier and a variable antialiasing filter for each channel followed by an analog-to-digital converter/multiplexer with a maximum sampling rate of 50 kHz. Data are sent as 12 bit words to a PDP 11/34 computer via a serial line transmitter of 1 Mbit/s for later processing.

The crossed hot-wire signals are corrected for temperature and mean density, when applicable. The uncertainty due to calibration and linearization has been analyzed and shows that this probe has a maximum yaw angle error of 2 deg, as long as the flow is not parallel, within 10 deg to one of the wires. In addition, a 1-deg positioning error of the whole probe system is expected. The uncertainty on velocity is 3%. The velocity in the stall cell has a pitch angle with respect to the plane of the wires and introduces an additional uncertainty.

Experimental Procedure and Data Processing

The experimental procedure involved the determination of the number of stall cells and their propagation velocity, velocity measurements with the hot wires in front of, behind, and on the rotor blade, and the development of the classical performance map $\phi - \psi_{TS}$.

The determination of number of cells and propagation velocity is performed by producing hot-wire probes at the same axial plane at different circumferential locations and determining the phase differences of the hot-wire traces and frequency of the phenomenon.[5] This technique could not provide an accurate result for the case of many stall cells. For this case the auto- and cross-correlation technique is applied to the signals and the result provides more evidence together with the on-rotor measurements for the number of cells.

The velocity is measured at five radial positions, i.e., 10, 30, 50, 70, and 90% of the blade height, by the stationary probes on both sides of the rotor. The ambiguity in the flow direction determination is inherent in probes built according to the crossed hot-wire principle. To resolve this, one has to adapt the sensor positioning according to operating conditions. The bisector of the crossed hot-wire sensor is directed at 45 or 75 deg from axial, the direction at 75 deg being chosen when reverse flow is expected, as, for example, in a stall cell.

The thermal tuft probe is mounted with its wires along the radial direction with wire 1 upstream. Placed in this position, the probe shows if the flow moves in the nominal direction or if the complex flow reversal occurs. The V-shaped sensor is positioned with one wire parallel to the axial direction. Compensation for the centrifugal effect on the wires is applied during the data reduction.

Table 1 Operating conditions for points A-H

Point	No. of cells	U_c/U, %	Passing frequency Hz	Stall
A			Clean flow	
E	8	84	113.0	Small perturbation
E′	7-10	—	—	Small perturbation
F	1	31	5.2	Deep stall
G	2	32	10.7	Deep stall
H	1	30	5.0	Deep stall

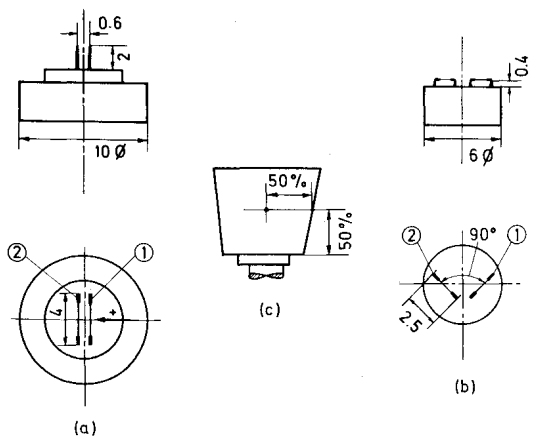

Fig. 2 Thermal tuft and V-shaped hot wire sensor.

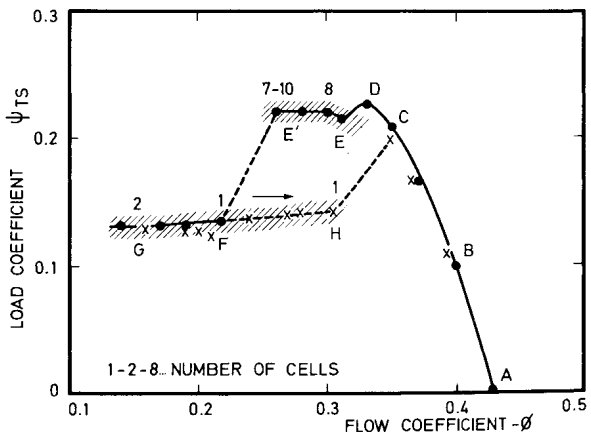

Fig. 3 Performance map.

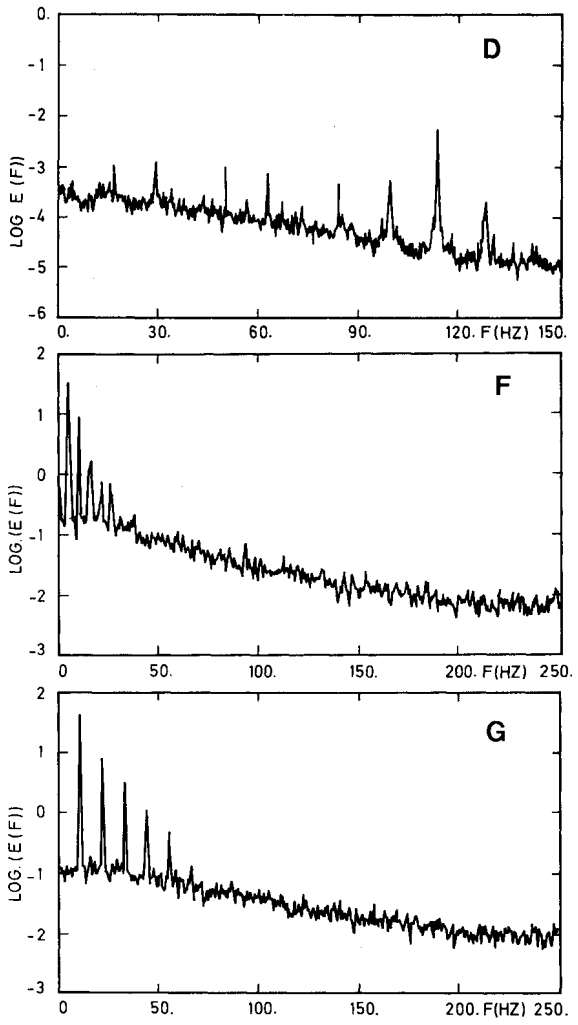

Fig. 4 Power spectra for three stall configurations.

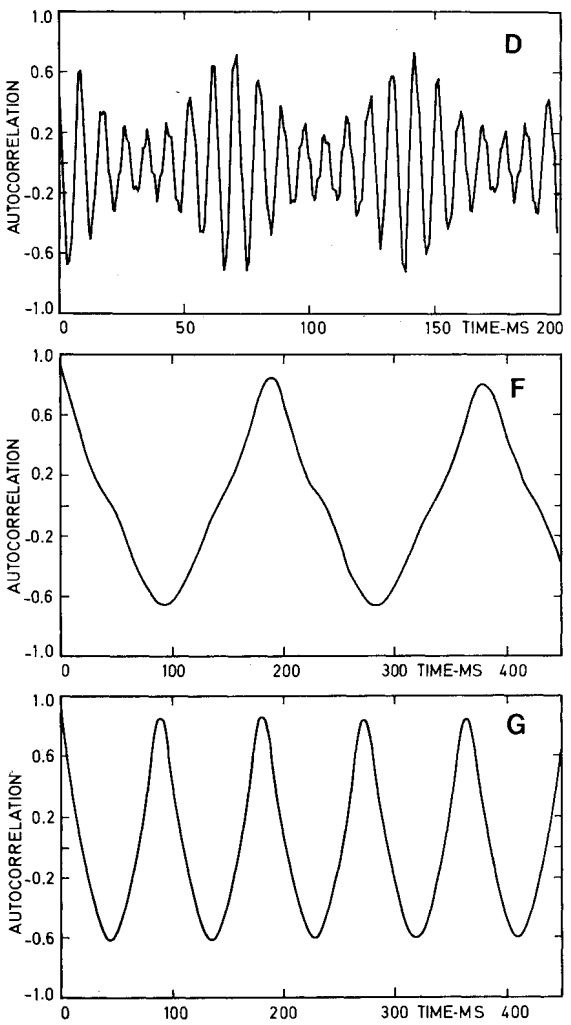

Fig. 5 Autocorrelations for three stall configurations.

Two different types of data sample are acquired to obtain the results presented herein. The first one is a set of 20 data strings with 1024 words/channel each at 300 or 500 Hz sampling frequency. They are used for power spectra calculation by means of a fast Fourier transform routine. The second type is a long sample of 14,336 words/channel at 6250 Hz sampling frequency for the stationary sensor and 3125 Hz for the rotating sensors. The sample is used for the instantaneous velocity and autocorrelation calculation. Averaged velocity and angle distributions and their fluctuations around the averaged values during a stall event are obtained with the aid of the phase-locked averaging technique. All tests are performed at 1000 rpm.

Results from Stationary Measurements

The stage performance map is obtained by radial flow surveys of the complete stage (Fig. 3). Operating conditions for points A→H on the map are summarized in Table 1.

The correlation from Ref. 8 indicated the occurrence of rotating stall and no surge based on the parameter B being smaller than 0.70. Full-span rotating stall is possible when the blockage due to the cells is more than 30% of the total annulus area. This is confirmed in experiments on a compressor model with $B=0.12$. The local (radial) and overall (annular) blockage factor λ is evaluated from the velocity measurements. The values $\lambda_1=0.42$ (one cell) and $\lambda_2=0.48$ (two cells) are well above 0.3 for which full-span cells are observed. The ψ_{TS} in stall (with the definition of Ref. 4) is close to 0.11, while ϕ_H equals 0.79 times the ϕ value on the stable characteristic at the same local coefficient $\psi_{TS\text{-}(H)}$.

Power Spectra and Autocorrelation

This analysis is performed to study the energy content in the fluctuating components at the different frequencies, the shape of the stall cell, the preservation with time, and correspondence from cell to cell.

The power spectra are calculated up to one-half the sampling frequency using the velocity signals and a fast Fourier transform. Log $[E(f)]$ is presented as a function of frequency where the calculations are performed with a frequency window f_s/N.

In the unstalled condition, A→C, only the rotor blade passing frequency is observed in the two measuring planes which was filtered from the test data at the other operating points. The power spectra for points D, F, and G are shown in Fig. 4. The dominating frequency for case D is 113 Hz or eight cells, with a seven- and nine-cell harmonic content at 113 ± 14 Hz. The one-cell pattern (point F) has the peak at 5.2 Hz with rapidly decaying harmonics due to the nonsinusoidal shape of the stall cell. The expansion of the scale in the low-frequency domain allows the exact definition of the period for the event. Similar observations can be made for point G or the two-cell structure at 10.7 Hz. The one cell in the return branch (point H) showed the same spectra as point F. From these spectra we observe that a substantial amount of energy is contained in the harmonics of the cell passing frequency.

The autocorrelations are identical for the velocity and angle signals and the results are shown for the points D, F, and G (Fig. 5). The operating points A→C showed the characteristic turbulent flow autocorrelation for unidirectional flowfield. The result for point D shows a modulated signal with the highest aurocorrelation every 70 ms and less strong every 8.8

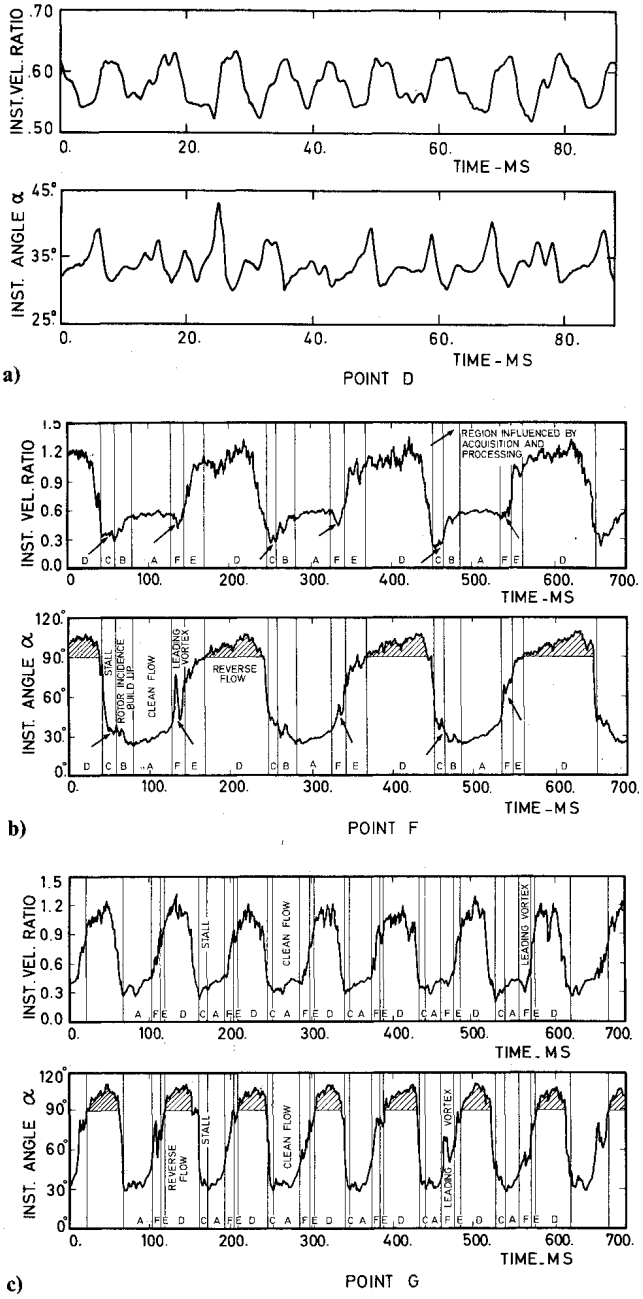

Fig. 6 Instantaneous velocity and flow angle for three stall configurations.

ms corresponding to a frequency of 113 Hz. The eight-cell pattern preserves itself well, but small cell-to-cell differences do exist within the pattern. A high level, ~0.85, exists for the aurocorrelation of the one and two cells at 195 and 91 ms, respectively. This confirms an almost invariant cell pattern with time and the close similarity of the cells in a two-cell configuration.

The Instantaneous Velocity Field

Examples of the upstream instantaneous velocity and flow angle variations for the eight, one, and two cells are shown at 70% of the blade height for the eight cells, 90% for the one, and 70% for the two cells (Fig. 6).

The eight-cell pattern (point D) shows oscillations of 14% around the average velocity level and ±5 deg around the average angle. The one cell (point F) occupies more than one-half the circumference and the flow direction is greater than 90 deg from axial 36% of the time, indicating reverse flow in that area. In the same region, the absolute flow velocity equals or surpasses the local rotor peripheral speed. This is explained by the local velocity triangle and the reverse flow in the rotating blades. The same behavior is seen in each cell for the two cells as well as for the one cell in the return branch. The time span of the unstalled flow is seriously reduced in the case of two cells.

The propagating cell moves at a fraction of the rotor speed and fixed instrumentation will sense the unstalled flow first, then the leading front of the cell, followed by the central part, and finally the trailing end as shown in the velocity-time diagram. The rotor, on the contrary, approaches the cell from the trailing end due to the larger peripheral velocity. Therefore, the leading edge of the rotating stall cell corresponds to the unstalling process of the compressor rotor blading, while stalling of the rotor occurs at the trailing end of the cell.

A local oscillation of the flow direction is observed when the cell leading edge passes a fixed instrument. This is seen in the case of a single- as well as a two-cell pattern. It is very distinct at radii near the tip. We interpret it as a vortex forming the leading front of 1½ blade passages or 10% of the cell extent. The trailing end of the cells also has an indication of these vortices but the steep gradient masks the effect. It is observed in all of the large samples but is attenuated in the averaging process due to small fluctuations in the cell extension. The theoretical analysis for the rotating stall described in Ref. 1 assumed that the airfoils lose or gain their circulation when entering or leaving stall by shedding vortices.

The analysis of the instantaneous and phase-locked averaged velocity and angle variations showed that a delay exists between velocity and angle variations, as has also been shown with cross-spectra calculations.

For point D, the velocity is delayed with respect to the angle by 2.5. ms. For deep stall, the angle shows a delay of 20 (point F) and 18 ms (point G) as measured on the instantaneous traces. The delay for points F and G is explained as follows: The flow between the rotor and the inlet guide vanes is first deflected and then accelerated until a velocity close to the peripheral blade speed is obtained during the sequence when the rotor blade approaches the stall cell. At the leading edge of the large cells, no phase difference between velocity and angle is observed in the unstalling process of the rotor blades. These phase differences are observed at all blade heights.

Structure of the Rotating Stall Cell

A detailed description of the stalling procedure for points F and G can be given. The different zones which can be distinguished are found by combining velocity and flow angle and relate the results to the rotor blade. It is useful to follow the trace in opposite direction to the time scale, A→D→F. Six zones are found (Fig. 6).

Zone A: Where the velocity is constant and the absolute flow angle is still adjusting itself to the clean flow condition.

Zone B: The velocity decrease and angle increase result in a buildup of the rotor blade incidence angle. An instantaneous incidence angle of 25 deg can be obtained during this unsteady condition.

Zone C: The absolute velocity remains at a very low level, the inlet flow angle suddenly increases to 90 deg, and permanent stall has occurred.

Zone D: The tangential flow from the rotor starts entraining the fluid in the IGV-rotor space at a velocity slightly above the peripheral speed and a large zone of reverse flow appears. This reverse flow region is centered toward the back end of the stall cell. In fact, it is fed by the rotor.

Zone E: As we move toward the cell leading edge, a decay of the rotor return flow occurs and the flow angle becomes smaller than 90 deg; the velocity follows a similar trend.

Zone F: This is the front or "head" of the rotating stall cell. The combination of velocity and angle variations suggests a vortex-type motion by which the flow around the rotor blades is restored to the clean flow condition.

The rotating stall cell can be defined by the zones [C, D, E, F]. Some of these zones are not always present at all radial

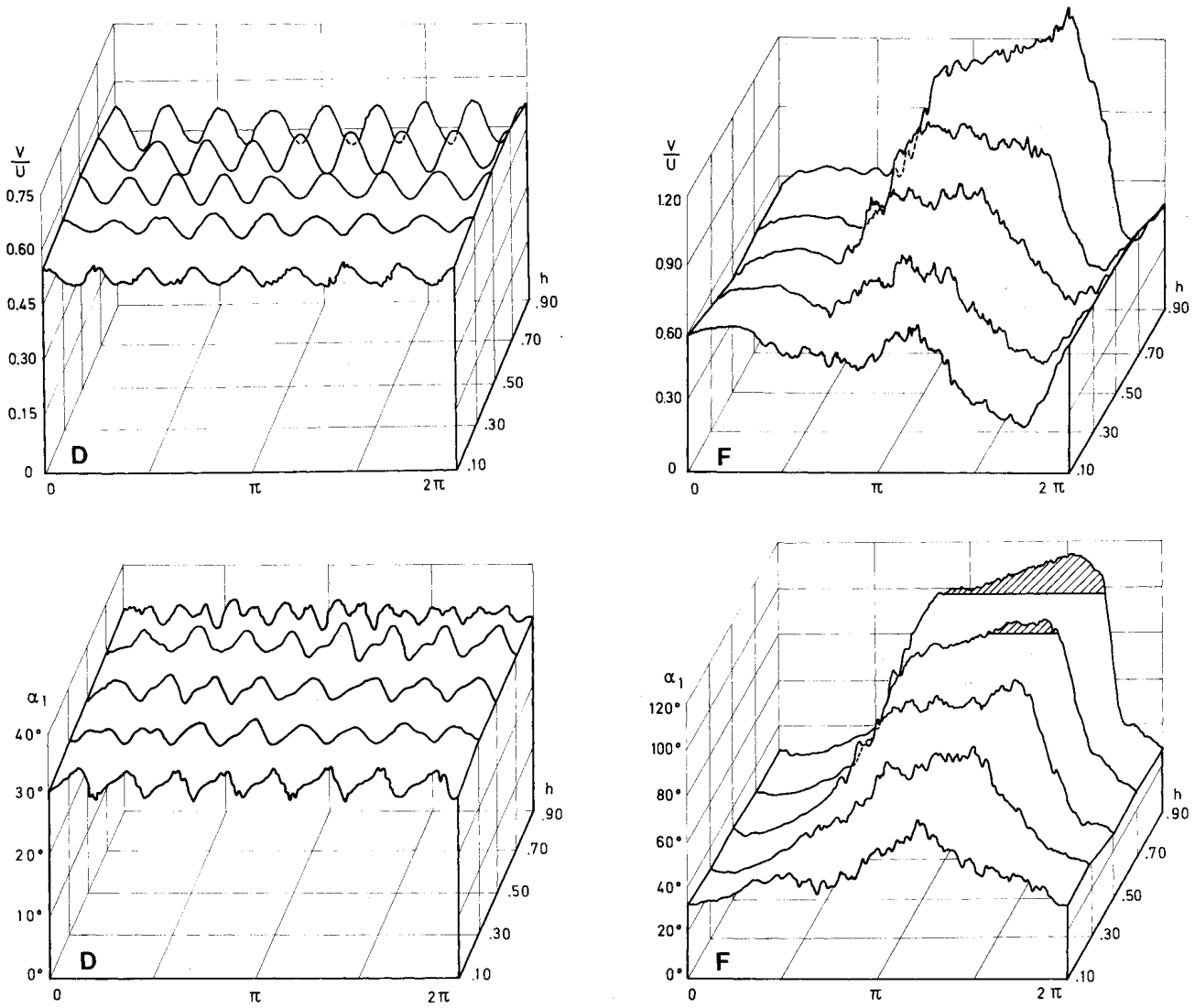

Fig. 7 Phase-averaged velocities and flow angles, inlet flowfield.

positions, others will be strongly attenuated or suppressed completely due to the sampling technique in the acquisition phase or the averaging technique in the data processing. The areas where this may occur are indicated by an arrow. According to this definition the rotating stall cell presented in this figure occupies 63% of the circumference. The two cells cover 65 or 60% of the tip circumference depending on the inclusion or not of the overlapping zones B and C. At other radial stations, where D disappears from the mean radius toward the hub, zone F is not as well defined near the hub and zones B and C are more spread out in this region of the blade.

Rotor Inlet Flowfield

The periodic variations of the incidence angle and velocity, the blade stall, flow reversal, and the rotating stall cell structure can be studied by the phase-locked averaged results for the velocity and angle variation during one stall event ($0 \rightarrow 2\pi$). This technique is used to eliminate random fluctuations from the signals and derive the pattern corresponding only to the periodic variations. The conditions for operating points D and F are given at five radial positions h. The conditions of points G and H can be found in Ref. 9.

Since the measurements at the different radial positions are not performed simultaneously, some synchronization of the different traces is needed. The alignment is done by using distinct features of the stall cell in the velocity or angle traces and centering them for the presentation. A sudden increase of angle at the leading and trailing edges of the cell, the center of the cell, and the clean flow zone have been used (Fig. 7).

The angle and velocity fluctuations are nearly sinusoidal and a well-organized eight-cell pattern can be observed, point D. The distinction between stalled and clean flow zones is difficult to make. No reverse- or high-flow angles occur. The amplitude of the velocity fluctuations decreases from 13 (tip) to 5% (hub) of the local velocity and the flow angle fluctuatons are ± 2 (tip) to ± 2.5 deg (hub) at an average flow angle of 32 deg from axial. The velocity maximum corresponds to the angle minimum and vice versa. The periodicity is better for the velocity traces and least for the angle variation near 70 and 90% of the channel height.

The stall cell region is characterized by high velocities and large flow angles in the one-cell case, point F. Reverse flow is present at the outer radii; these zones are indicated at 70 and 90% of the blade height as well as their tangential extension. The absolute velocity in the stall cell equals or exceeds the rotor peripheral speed. Near the hub, at 30 and 10% height, the flow angle reaches maximum values of 70 and 60 deg, respectively, and a small axial component is present. This cell can be viewed as propagating in the tangential direction, being fed at the outer radius by fluid returning from the rotor. This return flow executes a helicoidal motion and is found back at the inner radius where it contributes to a small mass flow influx into the rotor blades during the occurrence of rotating stall.

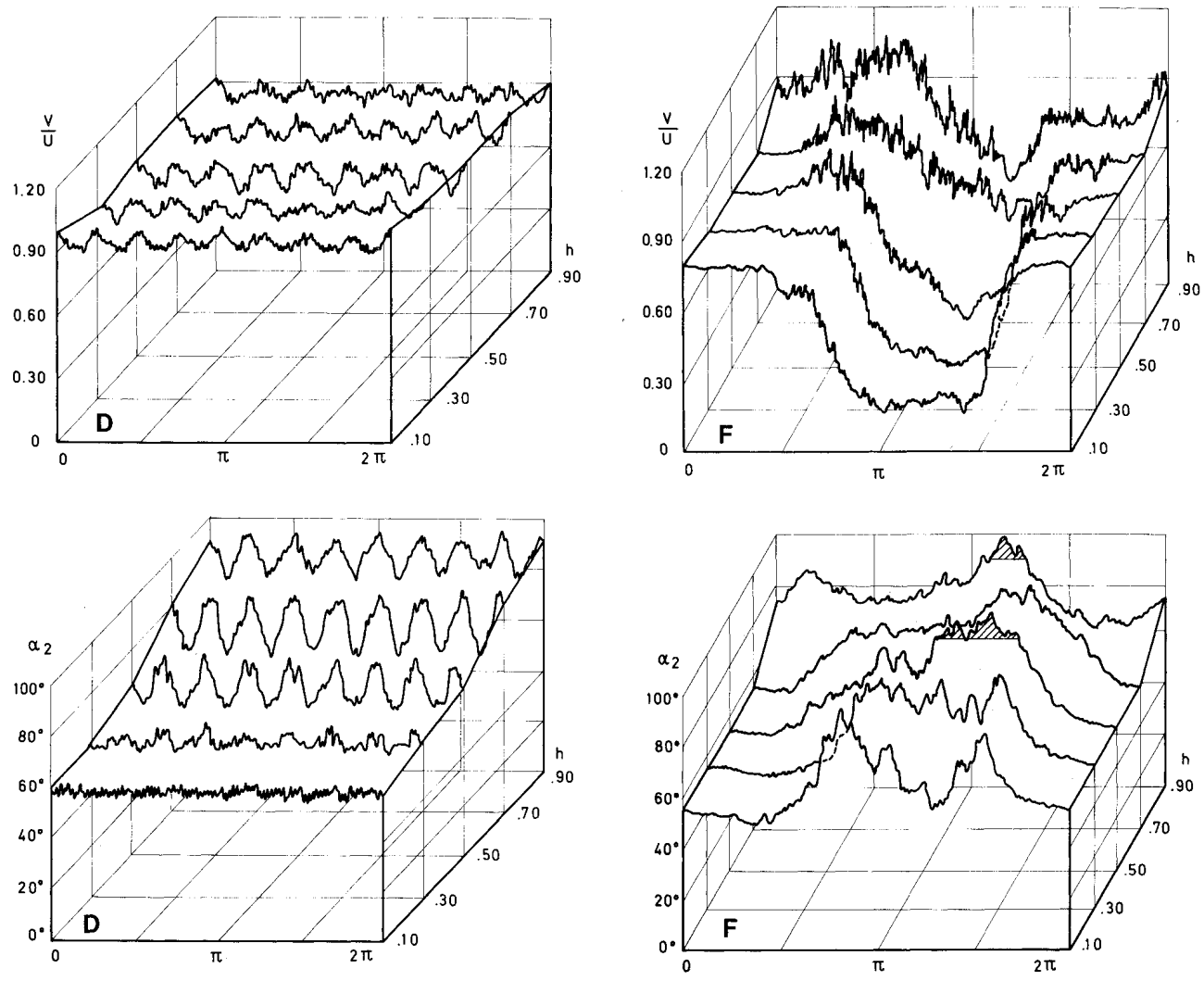

Fig. 8 Phase-averaged velocities and flow angles, outlet flowfield.

The pattern inside the cells for the points G and H is found to be similar to the one at point F.[9]

Rotor Outlet Flowfield

The nearly sinusoidal variation of velocity and flow angle are also observed in the downstream flowfield in the eight-cell flow pattern (point D) as seen in Fig. 8.

The averaging technique has not smoothed out all small perturbations. The exit flow direction is 58 deg near the hub and 85 deg at the tip radius. The angle fluctuations increase from hub to 70% height where ±12 deg are observed. The clean flow exit direction is 50 deg. The average velocity decreases from hub to tip. The eight-cell pattern is best observed in the upper 75% of the channel; the velocity fluctuations are of the same magnitude up- and downstream, whereas the angular variations are up to five times larger in the downstream field.

The one cell is characterized downstream by low velocities and high swirl angles at the cell location, corresponding to a separation on the rotor blade, point F. Reverse flow into the rotor is observed in the upper half on the channel height, but the circumferential extension is smaller than in the inlet flowfield. The clean flow part extension, marked very well in the lower half of the channel height, shrinks toward the tip radius as shown in the figure. The flow angle and velocity ratio in that region are 55-65 deg and 0.76, respectively. The large flow angle and velocity in the upper half yield relative flow directions with a small deviation from the rotor blade exit angle, but the relative velocity corresponds to such a large diffusion factor that flow separation is concluded to occur. The stall cell shows an abrupt evolution near the hub with constant velocity in the cell, while gradual evolution and still strongly varying velocities occur near the outer radius.

Results from on Rotor Measurements

Results obtained from the thermal tuft and V-shaped sensor are now presented. Information on the flow behavior is considered to be important because phenomena near the blade surface, e.g., flow separation, seem to play a dominant role in the occurrence and development of rotating stall.

Thermal Tuft Results

The measurements, in the relative frame of reference, must be interpreted by reading the traces in the opposite direction when a comparison has to be made with the absolute motion. The most interesting information from the sensor comes from the variation of the velocity ratio Ve_2/Ve_1.

The variation of this ratio for point F is given in Fig. 9. In the clean flow region the ratio is 0.2, not fluctuating much around this value. Inside the stall cell the values are strongly fluctuating around a mean of 0.45. From the performance characteristics of the thermal tuft, it is concluded that in the clean flow the meridional velocity has a direction close to axial which does not happen in the stall cell. The velocity ratio in the cell is increased but much lower than unity which means the flow is not reversed. It still moves in the positive direction but contains an important radial component.[10]

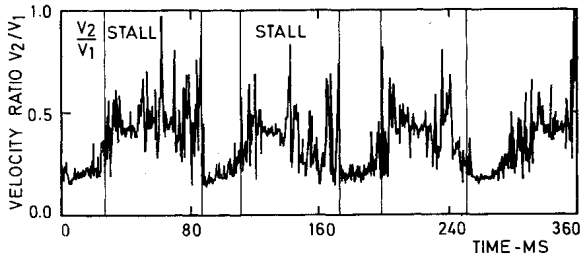

Fig. 9 Instantaneous velocity ratios from thermal tuft, one stall cell.

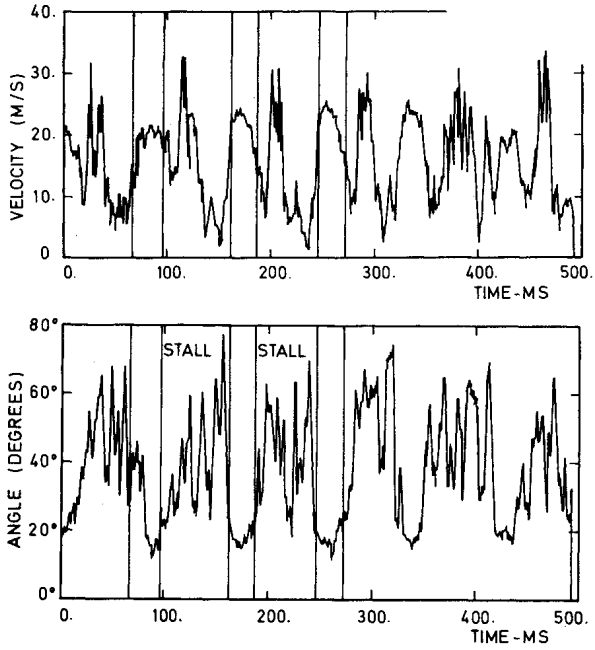

Fig. 10 Instantaneous velocity and angle from V-shaped sensor, one stall cell.

V-shaped Sensor Results

The measurements performed with the V-shaped hot-wire arrangement clarified the flow conditions at the midblade location. The local flow vector is almost in a horizontal plane at operating point A. A radial component is introduced as the diffusion in the blade channel increases and the radial drift in the boundary layer is observed at the location of the two wires.

For point F, the clean flow conditions correspond to 23 m/s and 18 deg unstalled meridional flow angle. The blade surface velocity drops when entering stall, subsequently increases to clean flow levels or higher, and finally drops to very low values. The unstalled conditions are restored abruptly. The meridional flow angles rises from 18 to 50 to 60 deg with a maximum of 70 deg, showing very high fluctuations (Fig. 10).

The flow is strongly three-dimensional and the radial velocity component is of the same magnitude as the axial one near the blade surface. This radially outward flow on the blades during stall is compatible with the reversed flow near the tip as shown in Fig. 7. This centrifugation of low-energy fluid is the link between the axial inlet flow in the cell near the hub and the reverse flow in the tip region.

Conclusions

Two different types of rotating stall have been identified.

1) A small stall consisting of small perturbations around the mean flow quantities. The performance of the compressor gradually drops and the flow continues to move through the rotor without significant radial reorganization.

2) A large stall consisting of one or two cells (in this case) with large velocity and angle variations. The performance drops abruptly and the flow through the rotor is completely reorganized in a three-dimensional manner with the appearance of reverse flow in front of the rotor.

In the case of large stall, the one and two cells appearing during throttling and the one cell in the hysteresis loop have identical structures.

Statistical analysis in the frequency and time domain showed that rotating stall is a periodic unsteady phenomenon well preserved in time.

A detailed description of the large stall cells, as seen from the stationary frame, is established based on the instantaneous flow pictures.

Measurements at midblade position on the suction surface of a rotor blade show that at that position flow reversal does not occur during large stall. A three-dimensional behavior at that point is confirmed. Radial velocities are small in the clean flow and found to be of the same order of magnitude as the axial velocity inside the stall cells, and large meridional flow angles occur. The low-energy fluid is centrifuged outward in the rotating blades.

References

[1]Kriebel, A. R., Seidel, B. S., and Schwind, R. G., "Stall Propagation in a Cascade of Airfoils," NASA TR R61, 1960.

[2]Takata, H. and Nagano, S., "Nonlinear Analysis of Rotating Stall," ASME Paper 72-GT-3, 1972.

[3]Orner, N., "Rotating Stall in Axial Flow Compressors," *Unsteady Flow in Turbomachines*, von Karman Institute for Fluid Dynamics, Rhode St. Genèse, Belgium, VKI LS 1979-3, February 1979.

[4]Day, I. J., Greitzer, E. M., and Cumpsty, N. A., "Prediction of Compressor Performance in Rotating Stall," ASME Paper 77-GT-10, 1977.

[5]Costilow, E. L. and Huppert, M. C., "Rotating Stall Characteristics of a Rotor with Hub-Tip Radius Ratio," NACA TN 3518, 1955.

[6]Day, I. J. and Cumpsty, N. A., "The Measurement and Interpretation of Flow within Rotating Stall Cells in an Axial Compressor," Cambridge University, CUED/A-Turb/TR 90, 1977.

[7]Gyles, B. R., Ligrani, P. M., and Breugelmans, F. A. E., "Rotating Stall in an Axial Flow Single Stage Compressor on Blade Velocity Measurements," AFOSR-80-0119B, April 1982.

[8]Greitzer, E. M., "Review—Axial Compressor Stall Phenomena," *ASME Transactions, Journal of Fluids Engineering*, Ser. I, Vol. 102, No. 2, June 1980, pp. 134-151.

[9]Breugelmans, F. A. E., Mathioudakis, K., and Casalini, F., "Flow in Rotating Stall Cells of a Low Speed Axial Flow Compressor," *6th International Symposium on Air Breathing Engines*, Paper 83-7073, June 1983, pp. 632-642.

[10]Ligrani, P. M., Gyles, B. R., Mathioudakis, K., and Breugelmans, F. A. E. "Sensor for Flow Measurements near the Surface of a Compressor Blade," Journal of Physics E: Scientific Instruments, Vol. 16, May 1983, pp. 431-437.